Laser Excited Electronic and Thermal Elastic Vibrations in a Semiconductor Rectangular Plate

D. M. Todorović[1], B. Cretin[2], P. Vairac[2], Y. Q. Song[3], M. D. Rabasović[4], D. D. Markushev[4]

[1] Institute for Multidisciplinary Researches, University of Belgrade, P.O.Box 33, 11030 Belgrade, Serbia,

[2] FEMTO-ST, Université de Franche-Comté, ENSMM, UTBM, Besançon, France

[3] MOE Key Lab for Strength and Vibration, School of Aerospace, Xi'an Jiaotong University, P.R.China

[4] Institute of Physics, Universiy of Belgrade, Belgrade-Zemun, Serbia

[1] To whom correspondence should be addressed. E-mail:dmtodor@afrodita.rcub.bg.ac.rs

Abstract

Photoacoustic (PA) and photothermal (PT) effects can be important as driven mechanisms for micromechanical structures, especially for micro-(opto)electro-mechanical structures (MOEMS). A new approach for producing compact, lightweight, a highly sensitive detector is provided by MOEMS technology, which are based on the the elastic bending of microstructure generated by absorption of modulated optical power. The electronic and thermal elastic vibrations (the electronic deformation and thermoelastic mechanisms of elastic wave generation) in a semiconductor rectangular simply supported plate (3D geometry), photogenerated by a focused and intensity-modulated laser beam, were studied. The theoretical model for the elastic displacements space and frequency distribution by using the Green function method was given. The amplitude of the elastic bending in the rectangular plate were calculated and analysed, including the thermalization and surface and volume recombination heat sources. The theoretical results were compared with the experimental data. These investigations are important for many practical experimental situation (atomic force microscopy, thermal microscopy, thermoelastic microscopy, etc) and sensors and actuators.

Keywords: Elastic bending; Electronic and thermal elastic vibrations; Micromechanical structures; Photoacoustic; Photothermal;

1 Introduction

The development of microsystem technologies (surface and bulk micromachining) resulted in the production of miniature sensors, actuators, resonators and electromechanical parts. One of main problem is the methods of characterization of these microstructures. The photoacoustic (PA) and photothermal (PT) science and technology extensively developed new methods for the investigation of micro (nano) – electro – mechanical - systems (MEMS, OEMS). The PA and PT effects can be important also as driven mechanisms for optically excited micromechanical structures.

The PT and PA effects in micromechanical structures are based on the photogeneration of electron-hole pairs, i.e. plasma waves, generated by the absorbed intensity-modulated excitation. Depth-dependent plasma waves contribute to the generation of periodic heat and mechanical vibrations, i.e. thermal and elastic waves. The thermal waves in the sample cause elastic vibrations, i.e. the thermoelastic (TE) wave generation. On the other hand, the photogenerated carriers produce periodic elastic deformation in the sample – the electronic deformation (ED). The TE and ED mechanism are two main mechanisms of elastic displacement (elastic bending) generation in optically driven MEMS (NEMS), OEMS, especially for optically driven microstructures for sensors and actuators.

The analysis of the thermoelastic (TE) and electronic deformation (ED) effects in micromechanical structures consists in modeling a complex system by simultaneous analysis of the coupled plasma, thermal and elastic wave equations. Todorović et al. [1-3], theoretically and experimentally investigated the TE and ED effects in micromechanical structures.

The theoretical analysis of the plasma and thermal effects in micromechanical structures consists in modeling a complex system by simultaneous analysis of the plasma and thermal wave equations. In previously published papers, the plasma, thermal and elastic fields in one-dimension (1D) micromechanical structures were theoretically and experimentally analyzed by Todorović et al. [1-3]. The plasma and thermal waves, i.e. the carrier-density and temperature space and frequency distribution in a rectangular plate (3D geometry), photogenerated by a tightly focused and intensity-modulated laser beam, were are analyzed in our previously papers [4].

In this work the electronic and thermal elastic vibrations, i.e. the electronic deformation (ED) and thermoelastic (TE) space and frequency elastic bending distribution (3D geometry) in a simply supported semiconductor rectangular plate, photogenerated by a tightly focused and intensity-modulated laser beam, are analyzed.

2 Electronic and Thermal Elastic Vibrations

2.1 Plasma, Thermal and Elastic Fields

The theoretical treatment enables quantitative accounts of the carrier density field, $n(\boldsymbol{r},t)$, temperature field, $T(\boldsymbol{r},t)$ and elastic displacement field, $\boldsymbol{u}(\boldsymbol{r},t)$. In the case of periodical excitation, with angular modulating frequency of the incident beam ω, the excess carrier-density can be assumed as $n(\boldsymbol{r},t)=\mathrm{Re}[N(\boldsymbol{r},\omega)\exp(i\omega t)]$, temperature $T(\boldsymbol{r},t)=\mathrm{Re}[T(\boldsymbol{r},\omega)\exp(i\omega t)]$, and elastic displacement $\boldsymbol{u}(\boldsymbol{r},t;\omega)=\mathrm{Re}[\boldsymbol{u}(\boldsymbol{r},t)\exp(i\omega t)]$, where $N(\boldsymbol{r};\omega)$, $T(\boldsymbol{r},\omega)$ and $\boldsymbol{U}(\boldsymbol{r};\omega)$ are complex values which define the amplitude and phase of the carrier, temperature and displacment fields, respectively.

The plasma (carrier-density) and thermal fields in an opaque rectangular Si plate with dimensions L_x , L_y , L_z (3D geometry), excited with a tightly focused and intensity-modulated laser beam (Dirac harmonic source) centered at (x_1 , y_1 , $z_1 = 0$), is analyzed in our previously published paper [4]. Fig.1 shows rectangular plate with a focused laser beam excitation and optical probe detection configuration and the coordinate system for calculating the carrier density, temperature and elastic bending. The carrier-density $N(x,y,z;\omega)$ and temperature $T(x,y,z;\omega)$ space and frequency distribution in the Si plate were calculated and use as a source term in the elastic bending equation.

2.2 Electronic and Thermal Elastic Deformations

Absorption of the optical energy in a semiconductor plate causes the various ED and TE effects. The photogenerated plasma can directly produce a local strain, which then generates elastic waves in the semiconductor. The electronic strain, $\varepsilon^{ED}(\boldsymbol{r};\omega)$ can be given vs. the excess carrier density, $\varepsilon^{ED}(\boldsymbol{r};\omega) \approx d_n N(\boldsymbol{r};\omega)$, where d_n is the coefficient of electronic elastic deformation (d_n denotes the pressure dependence on the band gap energy at a constant temperature). Than, the electronic elastic displacement $\boldsymbol{U}^{\boldsymbol{ED}}(\boldsymbol{r};\omega)$, using the strain-stress relations, can be given vs. the electronic deformation. Also, the thermal elastic displacement $\boldsymbol{U}^{\boldsymbol{TE}}(\boldsymbol{r};\omega)$, can be given vs. the thermoelastic strain $\varepsilon^{TE}(\boldsymbol{r};\omega) \approx \alpha_T T(\boldsymbol{r};\omega)$, where α_T is the coefficient of linear expansion. Since d_n is negative for silicon, it means that electronic strain and thermal expansion are opposite in sign; the generation of excess carriers causes a contraction of the material, while thermal heating results in an expansion. Than, the elastic displacement $\boldsymbol{U}(\boldsymbol{r};\omega)$ can be given as the sum of two components: $\boldsymbol{U}^{\boldsymbol{ED}}(\boldsymbol{r};\omega)$ and $\boldsymbol{U}^{\boldsymbol{TE}}(\boldsymbol{r};\omega)$.

2.3 Theory of the elastic thin plate

The elastic bending calculation for a thin rectangular plate, with a thickness L_z much smaller than the length L_x and width L_y ($L_z << L_x , L_y$) is given. One side of the plate is illuminated with an intensity-modulated laser beam (Fig.1). When the thickness of the elastic plate is much smaller then all other plate dimensions, it

is possible to suppose that the elastic deformation is approximately the same along the sample thickness. For that reason, it is possible to use the simple theory of the elastic thin plate to obtain the elastic bending.

In accordance with the elastic theory of thin plate, the elastic displacements $\boldsymbol{U} = \{U_x, U_y, U_y\}$ for the plate are:

$$U_x(x,y,z,t) \approx -(z-z_n)\frac{\partial W(x,y;\omega)}{\partial x}, \quad U_y(x,y,z,t) \approx -(z-z_n)\frac{\partial W(x,y;\omega)}{\partial y}, \quad U_z(x,y,z,t) \approx W(x,y;\omega), \tag{1}$$

where $W(x,y;\omega)$ is the displacement of the elastic neutral plane of the plate and z_n is the position of the neutral plane ($z_n = L_z / 2$).

2.3.1 Elastic Strain-stress Relations

The following equation connects the component of elastic strain and the bending:

$$\varepsilon_{ij}(x,y,z;\omega) = -(z-z_n)\frac{\partial^2 W(x,y;\omega)}{\partial x_i \partial x_j}. \tag{2}$$

Components of elastic strain, $\sigma_{ij}(x,y,z;\omega)$ as a function of the displacement $W(x,y;\omega)$, can be obtain from stress-strain relation.

$$\sigma_{xx}(x,y,z;\omega) = -\frac{E_Y}{1-\nu^2}\left((z-z_n)\left[\frac{\partial^2 W(x,y;\omega)}{\partial x^2} + \nu\frac{\partial^2 W(x,y;\omega)}{\partial y^2}\right] + (1+\nu)\left[\varepsilon^{TE}(x,y,z;\omega) + \varepsilon^{ED}(x,y,z;\omega)\right]\right), \tag{3}$$

$$\sigma_{yy}(x,y,z;\omega) = -\frac{E_Y}{1-\nu^2}\left((z-z_n)\left[\frac{\partial^2 W(x,y;\omega)}{\partial y^2} + \nu\frac{\partial^2 W(x,y;\omega)}{\partial x^2}\right] + (1+\nu)\left[\varepsilon^{TE}(x,y,z;\omega) + \varepsilon^{ED}(x,y,z;\omega)\right]\right),$$

$$\sigma_{xy}(x,y,z;\omega) = \sigma_{zy}(x,y,z;\omega) = -\frac{E_Y}{1-\nu}(z-z_n)\frac{\partial^2 W(x,y,z;\omega)}{\partial x \partial y},$$

where the second term in the bracket of the right-hand-side of the equation is the source term from the thermal and plasma waves, as a function of the temperature and carrier density distribution in the sample.

2.3.2 Elastic Bending Moments

Let us now introduce into the analysis the resultants of the state of elastic stress-bending moments $M_{ij}(x,y;\omega)$ for $i,j = x,y$. In the elastic theory of the thin plate, instead of the stresses or average value of stresses per thickness, the so-called cross-section moments are usually used. These elastic bending and torsion moments in thin plate are:

$$M_{xx}(x,y;\omega) = -B\left[\frac{\partial^2 W(x,y;\omega)}{\partial x^2} + \nu\frac{\partial W^2(x,y;\omega)}{\partial y^2} + (1+\nu)\underline{m}(x,y;\omega)\right],$$

$$M_{zz}(x,y;\omega) = -B\left[\frac{\partial^2 W(x,y;\omega)}{\partial y^2} + \nu\frac{\partial W^2(x,y;\omega)}{\partial x^2} + (1+\nu)\underline{m}(x,y;\omega)\right], \tag{4}$$

$$H_{xy}(x,y;\omega) = -B(1-\nu)\frac{\partial^2 W(x,y;\omega)}{\partial x \partial y},$$

where $B = E_Y L_z^3/(12(1-\nu^2))$ is the flexural rigidity of the plate and $\underline{m}(x,y;\omega)$ is the TE and ED moment generation term, i.e. the source term from the thermal and plasma waves.

2.3.3 Elastic Bending Equation

The equation for the deflection of the plate is:

$$\frac{\partial^2 M_{ij}(x,y,t)}{\partial x_i \partial x_j} = 0, \qquad (i,j = x,y)$$

Sustituting for $M_{ij}(x,y;\omega)$ their values from Eq.4, we arrive at the equation for vibrations of the plate:

$$\nabla^2\nabla^2 w(x,y,t) = -(1+\nu)\nabla^2 \underline{m}(x,y,t), \qquad \nabla^2 = \frac{\partial^2}{\partial x^2} + \frac{\partial^2}{\partial y^2}. \tag{5}$$

2.3.4 Elastic Green Function in a Simply Supported Plate

A concentrated unit force (impulsive, Dirac), $\delta(\mathbf{r} - \mathbf{r_o})$, acts at point $\mathbf{r_o} = (x_o, y_o, z_o = L_z/2)$ perpendicular to the middle plane.

$$\nabla^2\nabla^2 W^*(\mathrm{x}, \mathrm{y}|x_o, y_o) = -\frac{1}{B}\delta(\mathrm{x} - x_o)\delta(\mathrm{y} - y_o), \qquad \nabla^2 = \frac{\partial^2}{\partial x^2} + \frac{\partial^2}{\partial y^2}. \tag{6}$$

The function $W^*(x,y \mid x_o, y_o)$ denotes the deflection at the point (x,y), due to the action of a unit concetrated force at the point (x_o,y_o). For rectangular simply supported plate at the edges, the elastic Green function $W^*(x,y \mid x_o,y_o)$, is given as [5]:

$$W^*(x,y|x_o,y_o) = \frac{1}{B}\frac{4}{L_x L_y}\sum_{m=1}^{\infty}\sum_{n=1}^{\infty}\frac{1}{e_{mn}}\varepsilon_m(x)\,\varepsilon_n(y)\varepsilon_m(x_o)\,\varepsilon_n(y_o), \tag{7}$$

$$\varepsilon_m(x) = \sin(a_m x), \quad a_m = \frac{m\pi}{L_x}, \quad \varepsilon_n(y) = \sin(b_n y), \quad b_n = \frac{n\pi}{L_y}, \quad e_{mn} = a_m^2 + b_n^2, \quad (m,n = 1,3,\ldots)$$

where $\{\varepsilon_m(x)\}$ and $\{\varepsilon_n(y)\}$ are the complete orthogonal eigenfunction sets associated with the x and y direction.

Then, the quasistatic elastic bending:

$$\begin{aligned} W(x,y;\omega) &= -(1+\nu)B\int_0^{Lx} dx_o \int_0^{Ly} dy_o\ \underline{m}(x_o,y_o;\omega)\left(\frac{\partial^2}{\partial x_o^2} + \frac{\partial^2}{\partial y_o^2}\right)W^*(x,y|x_o,y_o), \\ &= (1+\nu)\frac{4}{L_x L_y}\sum_{m=1}^{\infty}\sum_{n=1}^{\infty}\frac{1}{e_{mn}}\varepsilon_m(x)\,\varepsilon_n(y)\,s_{mn}(\omega), \\ s_{mn}(\omega) &= \int_0^{Lx} dx_o \int_0^{Ly} dy_o\ \underline{m}(x_o,y_o,\omega)\,\varepsilon_m(x_o)\,\varepsilon_n(y_o), \end{aligned} \tag{8}$$

3 Analysis of the Elastic Vibrations

The theoretical model, derived in this work, enables to calculate and analyzed the 3D elastic displacement field i.e. it enables to study the electronic and thermal elastic vibrations in the optically excited plate.

For a semiconductor it is possible to define one plasma source of the elastic vibrations (the electronic elastic bending) and four different heat source for the elastic vibrations (the thermal elastic bending). For each source, using the Green method is possible to derive the appropriate relations for elastic bending components.

3.1 Plasma source

The electronic deformation component of elastic displacement:

$$W^{ED}(x,y;\omega) = (1+\nu)\frac{4}{L_x L_y}\sum_{m=1}^{\infty}\sum_{n=1}^{\infty}\frac{1}{e_{mn}}\varepsilon_m(x)\ \varepsilon_n(y)\, s^{ED}{}_{mn}(\omega)\ , \tag{9}$$

$$s^{ED}{}_{mn}(\omega) = \int_0^{Lx} dx_o \int_0^{Ly} dy_o\ \underline{m}^{ED}(x_o,y_o,\omega)\,\varepsilon_m(x_o)\,\varepsilon_n(y_o), \qquad \underline{m}^{ED}(x,y;\omega) = d_n\frac{12}{L_z{}^3}\int_0^{Lz}\left(z-\frac{L_z}{2}\right)N(x,y,z;\omega)\,dz,$$

3.2 Thermal sources

There are three main mechanisms in thermal wave generation, i.e. there are three thermal sources in semiconductors: the thermalization heat source, $Q^T(\mathbf{r},\omega)$, the bulk recombination source, $Q^{BR}(\mathbf{r},\omega)$ and two different heat sources at the plate surface $z=0$, $Q_1{}^{SR}(\omega)$ and $Q_2{}^{SR}(\omega)$ at the plate surfaces $z=L_z$.

The periodic temperature distribution, $T(x,y,z;\omega)$ in the plate can be given as a sum of four components: the thermalization, $T^{TZ}(x,y,z;\omega)$, surface recombination $T^{SR1}(x,y,z;\omega)$, $T^{SR2}(x,y,z;\omega)$ and bulk $T^{BR}(x,y,z;\omega)$ components of the temperature distribution, respectively. Then, the thermoelastic component of elastic displacement:

$$W^{TE}(x,y;\omega) = (1+\nu)\frac{4}{L_x L_y}\sum_{m=1}^{\infty}\sum_{n=1}^{\infty}\frac{1}{e_{mn}}\varepsilon_m(x)\ \varepsilon_n(y)\, s^{TE}{}_{mn}(\omega)\ , \tag{10}$$

$$s^{TE}{}_{mn}(\omega) = \int_0^{Lx} dx_o \int_0^{Ly} dy_o\ \underline{m}^{TE}(x_o,y_o,\omega)\,\varepsilon_m(x_o)\,\varepsilon_n(y_o),$$

$$\underline{m}^{TE}(x,y;\omega) = \alpha_T\frac{12}{L_z{}^3}\int_0^{Lz}\left(z-\frac{L_z}{2}\right)\left[T^{TZ}(x,y,z;\omega)+T^{SR1}(x,y,z;\omega)+T^{SR2}(x,y,z;\omega)+T^{BR}(x,y,z;\omega)\right]dz,$$

The electronic and thermal elastic vibrations were calculated for typical parameters of Si and dimensions: length L_x = 9000 μm, width L_y = 4500 μm and thickness of the Si plate L_z = 300 μm. The typical parameters of the Si used in these simulations are given in Table 1.

Figures 2, 3 and 4 show typical examples of the elastic bending for the simply supported rectangular plate (Si , <111> , 9 x 4.5 mm , 300 um); optical excitation with tightly focused beam, modulated at the

frequency f = 5 kHz, impinges at point $x_1 = L_x / 2$ = 4.5 mm, $y_1 = L_y / 2$ = 2.25 mm; detection at the point : $x_d = L_x / 2$, $y_d = L_y / 2$. Space ddistribution of the amplitude of elastic bending for the simply supported rectangular plate is given in Fig.2. Fig. 3 shows components of the elastic vibrations (the amplitude of elastic bending) along x-axis ($y = L_y / 2$). Fig. 4 shows the electronic deformation (ED), thermoelastic (TE) and sum (TE + ED) components of vibrations. Partially, TE component is the sum of four components (TE_ TZ + TE_ SR1 + TE_ SR2 + TE_ BR).

3.3 Comparing Theoretical and Experimental Results

The theoretical model was verified by comparing with the experimental results. The small optically excited elastic vibrations of the plate were measured with a laser probe [6,7]. The laser probe was an optical interferometer designed to measure the very small vibrations of the micromechanical structures. The small deflection can be detected below 0.1 picometer magnitude in accurate adjustment conditions. This nondestructive apparatus mainly include optical excitation (Nd:YAG laser, 532 nm, 200 mW), and optical probe detection (HeNe laser, 633 nm, 0.5 mW). The excitation laser beam is modulated with an acousto-optic modulator (AOM), and the response signal was measured with a lock-in amplifier (the frequency range is 2-70 kHz). The presented measurements results were the mean values of at least three measurements in the same conditions.

The elastic vibrations were detected at the center of the plate. Fig.5 shows typical experimental amplitude elastic vibration spectra for a Si plate (n-type, <111>, 500-1000 Ωcm, both surfaces polished), with the following dimensions: length L_x = 9 mm; width L_y = 4.5 mm; and thickness L_z = 300 μm. The experimental results were comapred with the theoretically calculated spectra by using the theoretical model given in this work, including the TE and ED components. Fig.5 shows the best fit of the theoretically calculated amplitude spectra with experimental one. The parameters for Si used in calculation of the fitted spectra are given in Table 1.

Comparing the theoretical and experimental results shows good agreement in the frequency range from 3 kHz to ~34 kHz (below the frequency of a small damped resonant mode). Below the frequency of 3 kHz there is small deviation of the theoretically fitted curve from the experimental one. This is the consequence of the acoustic noise which slump in the low frequency rang.

4 Conclusion

The theoretical model for the space and frequency distribution of the electronic and thermal elastic displacements in a semiconductor plate (3D geometry), photogenerated by a tightly focused and intensity-modulated laser beam, was given. The theoretical relations for 3D elastic bending, including the electronic

deformation and four thermoelastic components (the thermalization, surface and bulk recombination) of the elastic bending were derived. The amplitude of elastic vibrations in the simply supported rectangular plate were calculated and analysed. The analysis of the amplitude space distribution shows that the elastic displacements are not only significant around the focused laser excitation point. The analysis also shows that the transport parameters (the lifetime and surface recombination velocities of the photogenerated carriers) have significant influence to the elastic vibrations. The theoretical model was verified by comparing with the experimental results.

These results showed that the photothermal elastic vibration spectra are very convenient for investigation the mechanical characteristics of micromechanical structures. This investigation is in progress.

Acknowledgments

This work was supported in part by the Ministry of Sciences and Technology Development, Republic of Serbia (the authors: D. M. Todorović, M. D. Rabasović, D. D. Markushev; the project ON161017).

References

1. D.M.Todorović, Rev. Sci.Instrum., **74** (1), 578 (2003)
2. Y. Song, B. Cretin, D. M. Todorović, P. Vairac, J. Phys. D: Appl. Phys. **41,** 155106 (2008)
3. D. M. Todorović, B. Cretin, Y. Song, P. Vairac, J. Appl. Phys., **107**, 023516 (9p) (2010)
4. D. M. Todorović Y. Song , J. Phys.: Conf. Ser., **214**, 012104 (2010)
5. W.Nowacki, *Thermoelasticity*, (Pergamon Press, Oxford, 1962)
6. B. Cretin, P. Vairac, Appl. Phys. Lett., **71**(15), 2083 (1997)
7. P. Vairac, B. Cretin, A. J. Kulik, Appl. Phys. Lett., **83**(18), 3824 (2003)

Table 1 Parameters and values

Parameter	symbol	value	unite
density of Si	ρ	$2.33 \cdot 10^{3}$	$kg \cdot m^{-3}$
optical reflectivity of Si	R_s	0.30	
optical absorption coefficient of Si	α	$5.00 \cdot 10^{5}$	m^{-1}
thermal conductivity of Si	K	150	$W \cdot m^{-1} . \cdot K^{-1}$
thermal conductivity of the air	K_q	0.025	$W \cdot m^{-1} . \cdot K^{-1}$
thermal capacity of Si	C	695	$J \cdot kg^{-1} . \cdot K^{-1}$
thermal difusivity of Si	D_T	$9.26 \cdot 10^{-5}$	$m^{2} . \cdot s^{-1}$
power of optical excitation	P_o	0.1	W
excitation energy	E	2.33	eV
energy gap of Si	E_G	1.11	eV
lifetime of photogenerated carriers	τ	$5.0 \cdot 10^{-6}$	s
coefficient of carrier diffusion for Si	D_E	$3.5 \cdot 10^{-3}$	$m^{2} \cdot s^{-1}$
recombination velocitie of the front surface	s_1	3	$m \cdot s^{-1}$
recombination velocitie of the rear surface	s_2	6	$m \cdot s^{-1}$
quantum efficiency of carrier genation	γ_G	1	
coefficient of bulk carrier recombination	γ_R	1	
Young's modulus for Si	E_Y	$1.31 \cdot 10^{11}$	$N \cdot m^{-2}$
linear thermal expansion for Si	α_T	$3.0 \cdot 10^{-6}$	K^{-1}
coefficient of electronic deformation	d_n	$-9.0 \cdot 10^{-31}$	m^{3}

Figure Captions

Fig. 1 Rectangular simply supported plate with a focused laser beam excitation and optical detection configuration and the coordinate system for calculating the carrier density, temperature and elastic bending

Fig. 2 Distribution of elastic vibrations (the amplitude of elastic bending) for the simply supported rectangular plate (Si , <111> , 9 x 4.5 mm , 300 um) ; optical excitation with tightly focused beam, modulated at the frequency f = 5 kHz, impinges at point $x_1 = L_x / 2$ = 4.5 mm, $y_1 = L_y / 2$ = 2.25 mm; detection at the point : $x_d = L_x / 2$, $y_d = L_y / 2$

Fig. 3 Components of elastic vibrations (the amplitude of elastic bending) along x-axis ($y = L_y / 2$) for the simply supported rectangular plate (Si , <111> , 9 x 4.5 mm , 300 um) ; optical excitation with tightly focused beam, impinges at point $x_1 = L_x / 2$ = 4.5 mm, $y_1 = L_y / 2$ = 2.25 mm; detection at the point : $x_d = L_x / 2$, $y_d = L_y / 2$: (red) bulk recombination component of the thermoelastic bending (TE_ BR); (blue) electronic deformation (ED); (green) surface recombination at the surface z = 0 (TE_ SR1) and $z = L_z$ (TE_ SR2); (yelow) termalization component (TE_ TZ); (x) sum of components (SUM)

Fig. 4 Electronic and thermal components of vibrations (the amplitude of elastic bending) vs. modulation frequency for the simply supported rectangular plate (Si , <111> , 9 x 4.5 mm , 300 um) ; optical excitation with tightly focused beam, impinges at point $x_1 = L_x / 2$ = 4.5 mm, $y_1 = L_y / 2$ = 2.25 mm; detection at the point : $x_d = L_x / 2$, $y_d = L_y / 2$: (- -) TE component (sum of TE_ TZ + TE_ SR1 + TE_ SR2 + TE_ BR); (-.-) ED component; (-.-) SUM (TE + ED)

Fig. 5 Amplitude of vibrations (elastic bending) vs. modulation frequency for the simply supported rectangular plate (Si , <111> , 9 x 4.5 mm , 300 um) ; optical excitation with tightly focused beam, impinges at point $x_1 = L_x / 2$ = 4.5 mm, $y_1 = L_y / 2$ = 2.25 mm; detection at the point : $x_d = L_x / 2$, $y_d = L_y / 2$: (x) experimental; (-) theoretically fitted

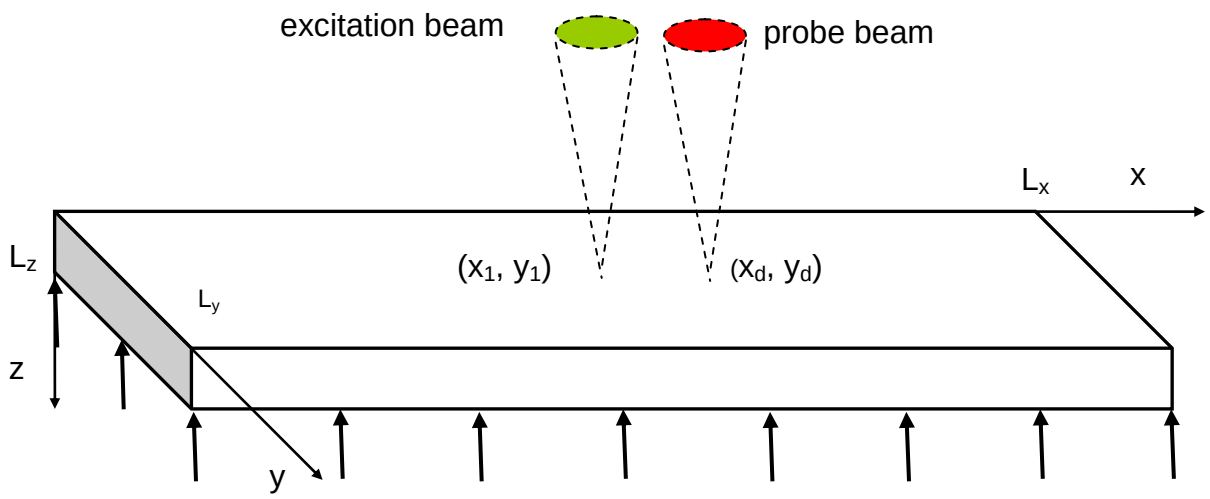

Fig. 1

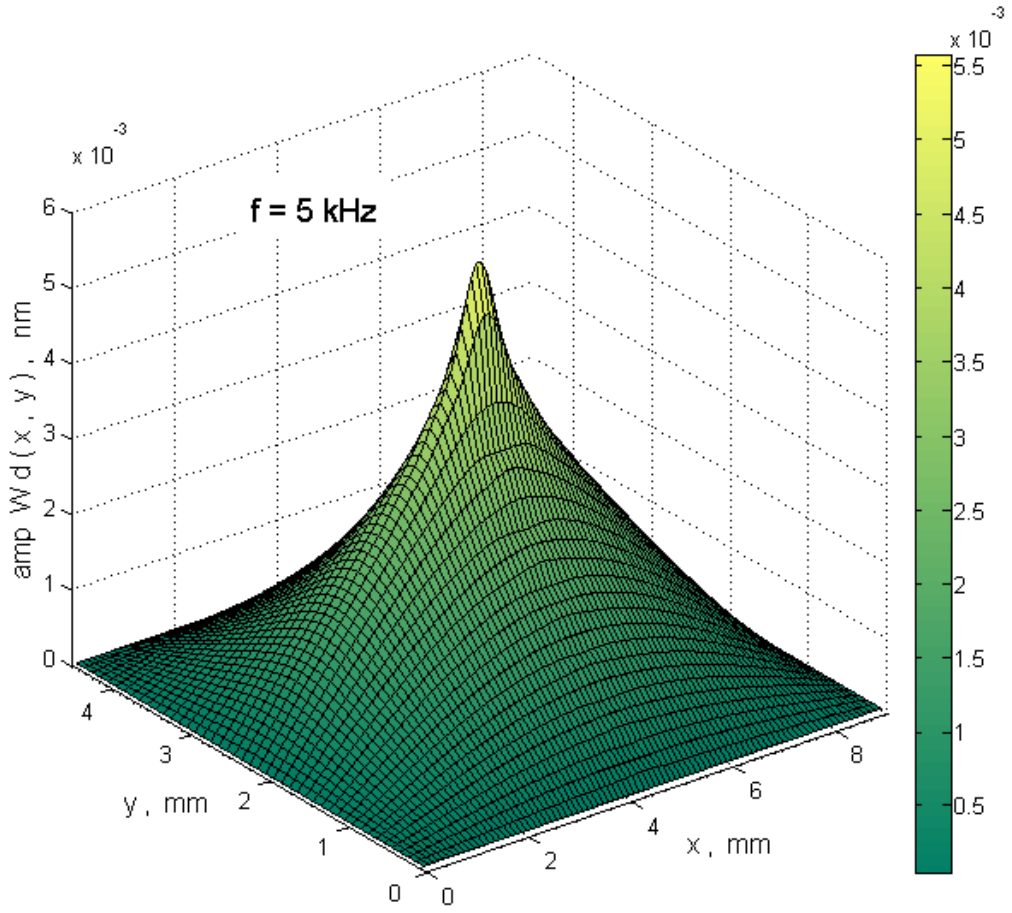

Fig. 2

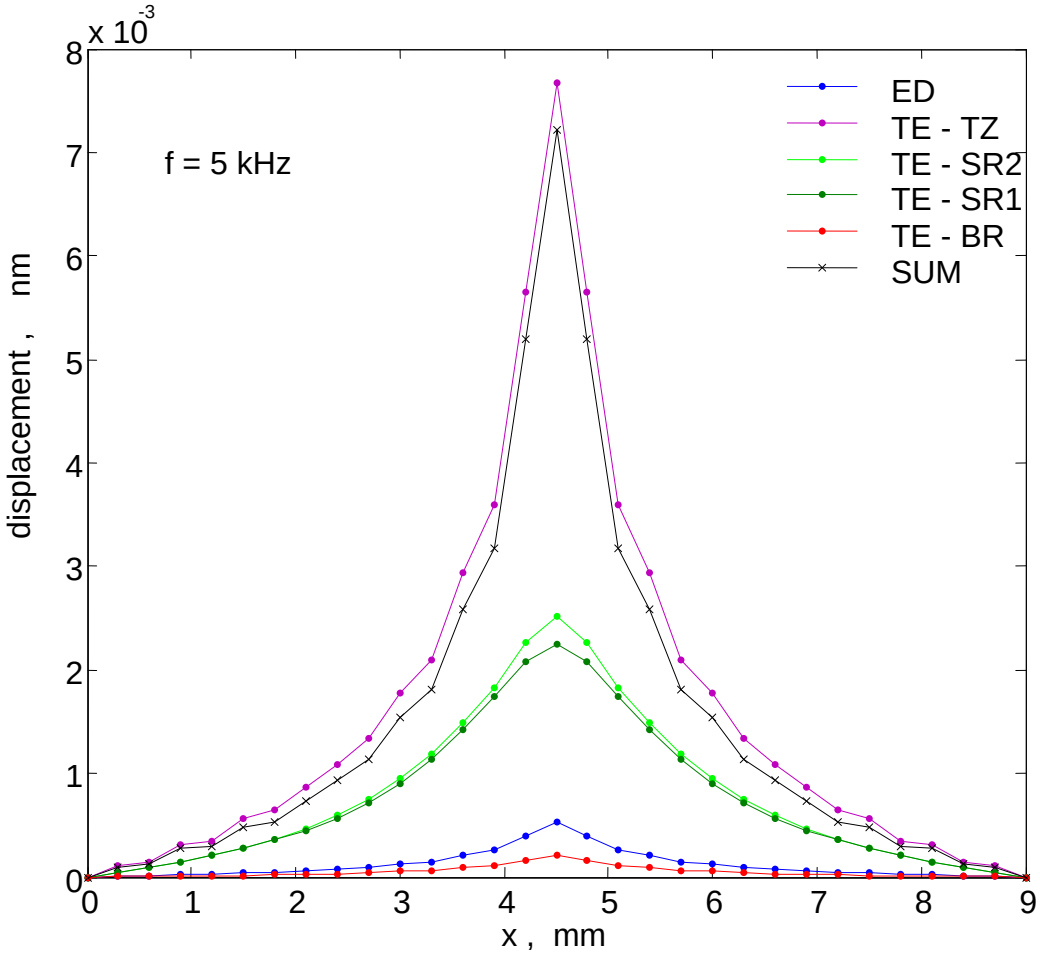
x 10^-3
f = 5 kHz
displacement , nm
x , mm
ED
TE - TZ
TE - SR2
TE - SR1
TE - BR
SUM
0
1
2
3
4
5
6
7
8
9

Fig. 3

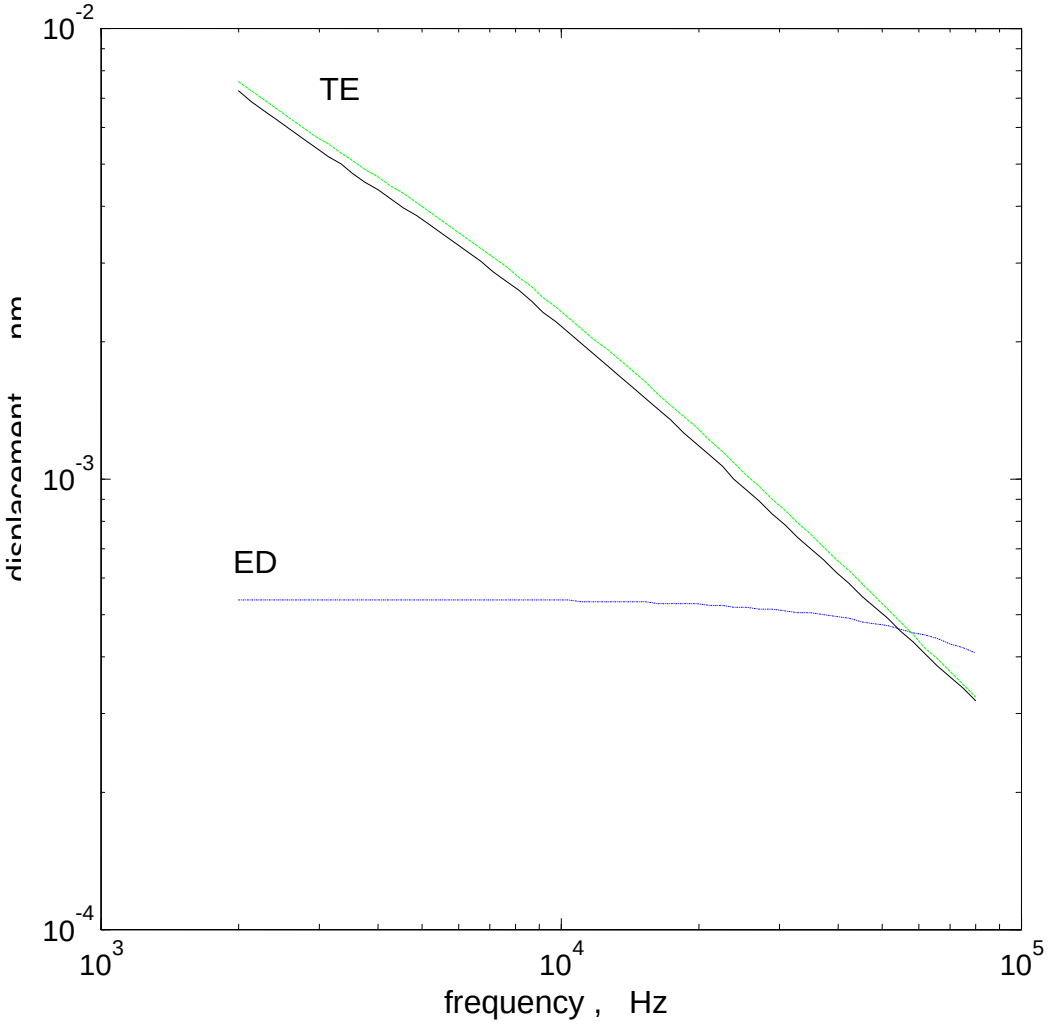

Fig. 4

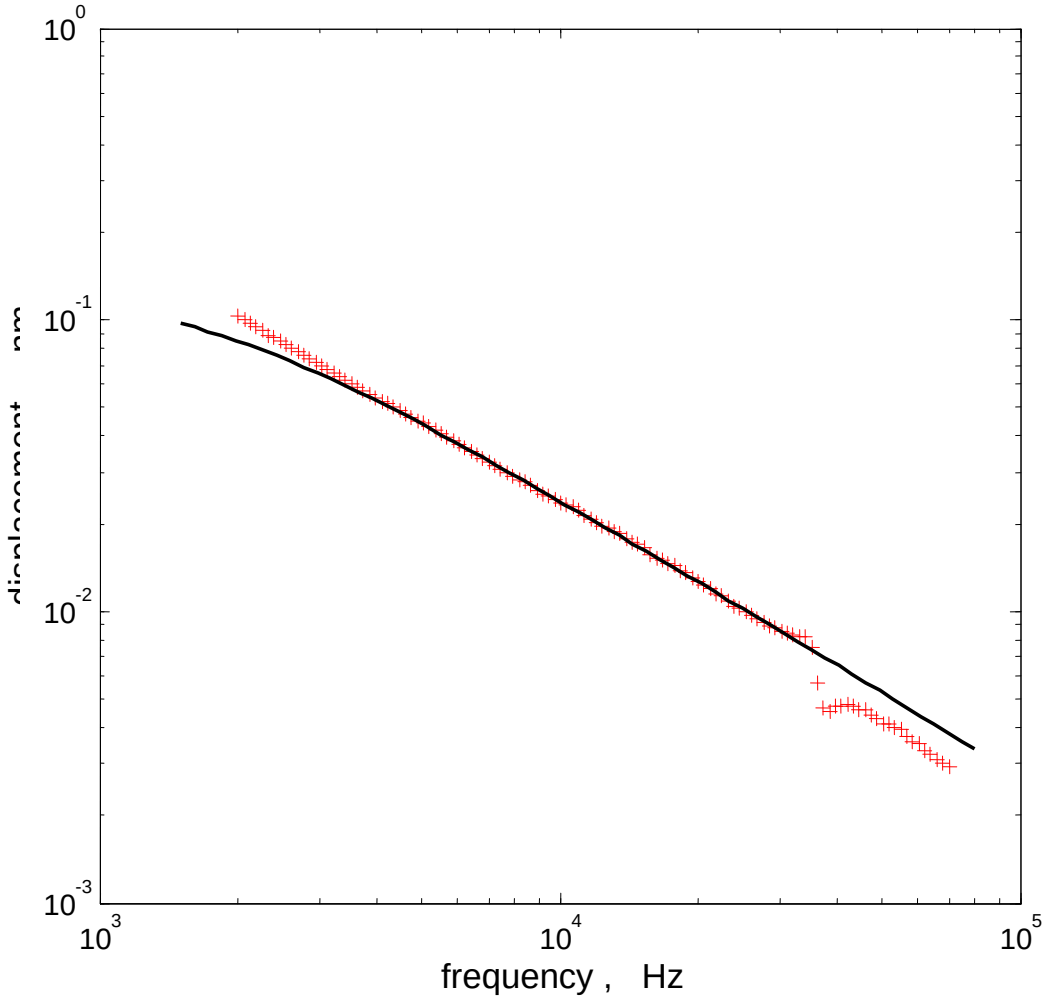

Fig. 5